

A Review and Comparison of Hysteresis Models for Magnetostrictive Materials

Sina Valadkhan
Graduate Student
Mechanical Engineering

Kirsten Morris
Professor
Applied Math Department

Amir Khajepour
Professor
Mechanical Engineering

University of Waterloo
Waterloo, Ontario N2L 3G1

Submitted to: Journal of Intelligent Material Systems and Structures
Professor Dan Inman, Editor
Department of Mechanical Engineering
310 Durham Hall
Virginia Polytechnic Institute and State University
Blacksburg, VA 24061, USA

Submission Date: January 11, 2006

Number of Pages: 20

Number of Figures: 16

Contact Author: Amir Khajepour
University of Waterloo
Department of Mechanical Engineering
Waterloo, Ontario N2L 3G1
CANADA
Tel: 519 888-4567 x6159
Fax: 519 888 4333
Email: akhajepour@uwaterloo.ca

A REVIEW AND COMPARISON OF HYSTERESIS MODELS FOR MAGNETOSTRICTIVE MATERIALS

Sina Valadkhan, Department of Mechanical Engineering,
University of Waterloo, email: svaladkh@uwaterloo.ca

Kirsten Morris, Department of Applied Mathematics,
University of Waterloo, email: kmorris@birch.math.uwaterloo.ca

Amir Khajepour, Department of Mechanical engineering,
University of Waterloo, email: akhajepour@uwaterloo.ca

ABSTRACT

In this article, the modeling of magnetostrictive materials is studied. Magnetostrictive materials become longer in the presence of a magnetic field, and are used mostly as actuators. These materials are highly nonlinear, and hence, very difficult to control. Here, Terfenol-D, a magnetostrictive material is studied. A setup has been designed to measure different parameters of a Terfenol-D sample. Using experimental data, the classical Preisach model, a physical variation of the Preisach model, and the Jiles-Atherton model are evaluated. For each model, the parameters are fine-tuned for Terfenol-D. The ease of use and accuracy of the models in the prediction of Terfenol-D behavior are compared.

1. INTRODUCTION

In recent years, a growing demand for micropositioning devices has been seen in industry. Micropositioning actuators are now commonly used in optical fiber alignment, biological cell micromanipulation, scanning microscopes and chip manufacturing. Currently, most of the micropositioning actuators are made of piezoceramic materials because of their fast response time and linearity.

There are demands for actuators with more force, larger stroke and faster response. For this purpose, the possibility of using other active materials for actuation is being examined. Among possible choices, Terfenol-D is a competitive choice. Terfenol-D, a magnetostrictive material, is an alloy of Iron, Terbium and Dysprosium. In comparison with other active materials, it has a very large force and displacement with a fast response time which makes it suitable for high-frequency applications.

In spite of its superior response, its application is less common in micropositioning devices. Terfenol-D, like other magnetic materials, has hysteresis. This nonlinearity and hysteresis makes it difficult to control. For this purpose, extensive research in hysteresis modeling is underway. Since in many micropositioning tasks, sub-micron accuracy is required, an accurate hysteresis model and control system is required if Terfenol-D is to be used for micropositioning applications.

Most of the literature for magnetostrictive hysteresis modeling is based on two main models: the Preisach model and the Jiles-Atherton model. The Preisach model is one of the earliest hysteresis models. This empirical model was developed in 1935 for magnetic

materials [1]. The Preisach model is explained in detail in [2]. In this model, the output is the weighted sum of the output of a continuum of hysteresis relays. The weight function for the relays depends on the material and needs to be identified. The Preisach model has been applied to many hysteretic systems, e.g. [3, 4, 5]. Many variations of this model have been developed.

In [3], an energy-based version of the Preisach model is introduced. Unlike the classical Preisach model, this model is derived from a physical model of magnetic materials. In this model, the system equilibrium points are found by modeling the Helmholtz free energy for each dipole. This model is classified as a Preisach model. The weight function is no longer an arbitrary function, but an exponential function with a few free parameters. Experimental data is used to fine tune these parameters. In [6], this model was extended to generalized weight functions. This extension improves the accuracy of the model.

In [7], the Preisach model is combined with a linear system to develop a hysteresis model for Terfenol-D that includes dynamical effects. In this model, a generalized weight function is used with an iterative identification algorithm. Experimental data and model results are compared at different frequencies.

As stated before, the weight function for the Preisach model depends on the system and must be identified with experimental data. Several identification algorithms have been proposed for this task. In [8], the identification problem is reformulated using a least-squares technique. In [9], this approach is examined in more detail for ferroelectric materials.

There are many implementations of the Jiles-Atherton model [10] for magnetostrictive materials. In the Jiles-Atherton model, the main magnetization mechanism is domain wall motion. Using an energy analysis, reversible and irreversible component of magnetization are modeled and a differential equation formulation for the system is obtained. This model has a few parameters to be identified. A major weakness of the Jiles-Atherton model is that it does not accurately reproduce the hysteresis curves in complex cases. This issue is fully discussed later in this paper.

In [11, 12], the Jiles-Atherton model is extended. It is suggested that the effects of stress for magnetostrictive materials can be represented with an additional magnetic field. In [12], the Jiles-Atherton model with quadratic magnetostriction is used. The effect of stress on magnetization is also modeled. The model results are compared with experimental data from a Terfenol-D sample.

The outline of this paper is as follows: In the next section, the test rig used to obtain experimental data is described. The experiments and data interpretation procedures are explained. It is shown that due to a relation between magnetization and elongation, the models only need to reproduce the magnetization. The Preisach model, its identification algorithm and model validation are included in Section 3. Section 4 covers the physical Preisach model and its identification and validation by experimental data. In Section 5,

the Jiles-Atherton model and the algorithm used for proper minor loop handling are explained. The various models are compared in the final section.

2. EXPERIMENTAL APPARATUS AND DATA COLLECTION

A test rig was designed to measure different parameters of Terfenol-D under different stresses and magnetic conditions. This test rig is shown in Figure 1. A Terfenol-D rod is surrounded by a magnetic coil in the actuation unit. The rod and coil are enclosed in a cylinder. An optical encoder with a resolution of 10nm measures the displacement produced by the actuation unit. A set of washer springs are used to load the actuation unit. The applied force is measured with a load cell and can be adjusted with a bolt on top of the setup. A frame made of aluminium is used to hold different parts of the setup together. Aluminium was chosen because of its neutral magnetic properties, resulting in no interference with magnetic components.

Terfenol-D cannot resist tension and should only be used in compression. This compression is supplied by the washer springs. The springs are soft enough so it can be assumed that the compression force is constant when the Terfenol-D changes size. The coil inside actuation unit is connected to a power supply controlled by a computer. There is a pickup coil in the actuation unit which measures the flux density inside the Terfenol-D rod. Two temperature sensors measure the coil and Terfenol-D rod temperature. The coil temperature is measured to make sure that it is not overheated and the Terfenol-D rod temperature is measured to compensate for any effects of thermal expansion. It was observed that the temperature rise in each experiment is less than 1°C and hence negligible. The current in the magnetic coil is measured in the power supply unit.

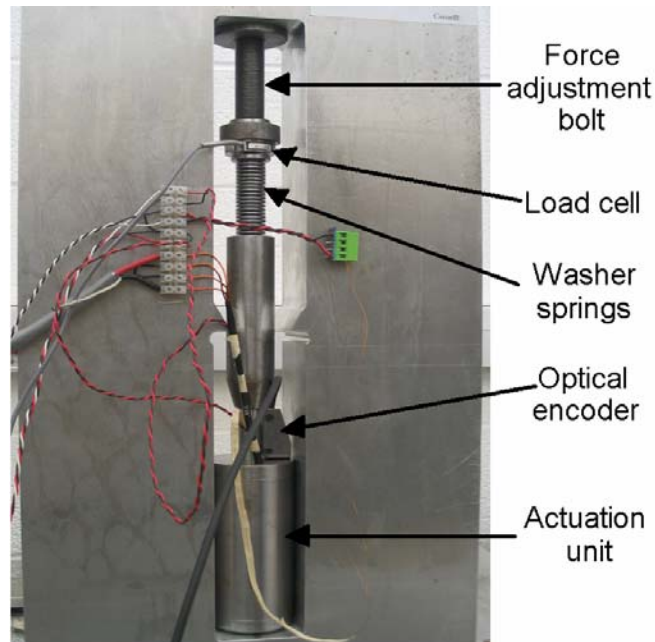


Figure 1: The experimental setup

This setup is used to obtain the relation between magnetic field H and magnetization M experimentally inside the Terfenol-D rod. The magnetic field H is controlled by the coil current and is considered to be the hysteretic system input. The magnetization M is a function of the magnetic field H and it is considered to be the output. Neither of these parameters is directly measurable.

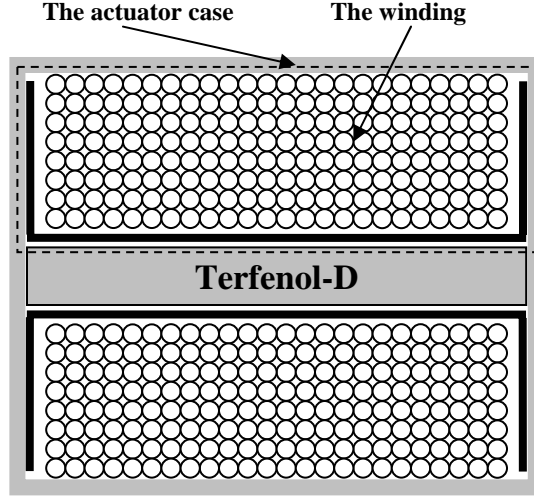


Figure 2: The magnetic circuit path.

To find the magnetic field H , the magnetic circuit for the actuation unit needs to be analyzed. Fig. 2 shows a cross-section of the actuation unit. The magnetic circuit path is shown with dashed line. As shown in this figure, the magnetic circuit path goes through the Terfenol-D rod and is completed by the actuator case. Ampere's law for this magnetic circuit can be written as:

$$ni = \oint H \cdot dl = \int_{case} H \cdot dl + H_{TD}l \quad (1)$$

where l is the length of Terfenol-D rod, H_{TD} is the magnetic field inside the Terfenol-D sample, i is the electrical current and n is the number of turns of the winding. If $\int_{case} H \cdot dl$ is known, one can use Equation (1) to compute the magnetic field H inside the Terfenol-D rod. Since the flux density B is measured by the pickup coil, the following equation can be used to compute magnetization M :

$$B = \mu_0(H + M). \quad (2)$$

To find $\int_{case} H \cdot dl$, the hysteresis relation for the actuator case must be known. A set of experiments was performed with the Terfenol-D rod replaced by a rod of cold rolled steel with known magnetic properties. In this case, Ampere's law can be written as:

$$ni = \oint H \cdot dl = \int_{case} H \cdot dl + H_{sample}l. \quad (3)$$

Using the magnetic properties, H_{sample} can be computed by looking up in the hysteresis curve. Now Equation (3) can be used to obtain $\int_{case} H \cdot dl$. It was found that $\int_{case} H \cdot dl$ is small compared to $H_{TD}l$ (more than ten times smaller), that is, the computed magnetic field H is only slightly modified if $\int_{case} H \cdot dl$ is assumed to be zero.

When a magnetostrictive material is in a magnetic field H , in addition to magnetization, elongation is also seen. Both elongation and magnetization are also affected by the mechanical stress applied to the material. For most magnetostrictive materials under a constant stress, there exists a simple relation between magnetization M and elongation λ . Fig. 3 shows the elongation versus magnetization for all experimental data when the stress is 1.04KSI. It is seen that, ignoring experimental errors, an algebraic relation exists between the elongation λ and M which is independent of system history. The similarity between Fig. 3 and a parabola suggests that the function $\lambda(M)$ can be approximated by a polynomial function of even powers of M [13]:

$$\lambda(M) = \gamma_2 M^2 + \gamma_4 M^4 + \dots \quad (4)$$

where parameters γ_2 and γ_4 depend only on stress. Usually the terms higher than γ_4 are not used. For the experimental data shown in Fig. 3, numerical values of γ_2 and γ_4 are: $\gamma_2 = 3.374 \times 10^{-15} (m/A)^2$ and $\gamma_4 = -1.9566 \times 10^{-27} (m/A)^4$. In Fig. 3, the curve given by equation (4) is shown with a dashed line. This dashed line lies among the experimental data and cannot be clearly seen, which shows an excellent agreement between the curve and the experimental data. The relation $\lambda(M) = \gamma_2 M^2$ represents the magnetization-elongation relation with good accuracy. The elongation λ is measured by an encoder and magnetization M is obtained experimentally using equation (2).

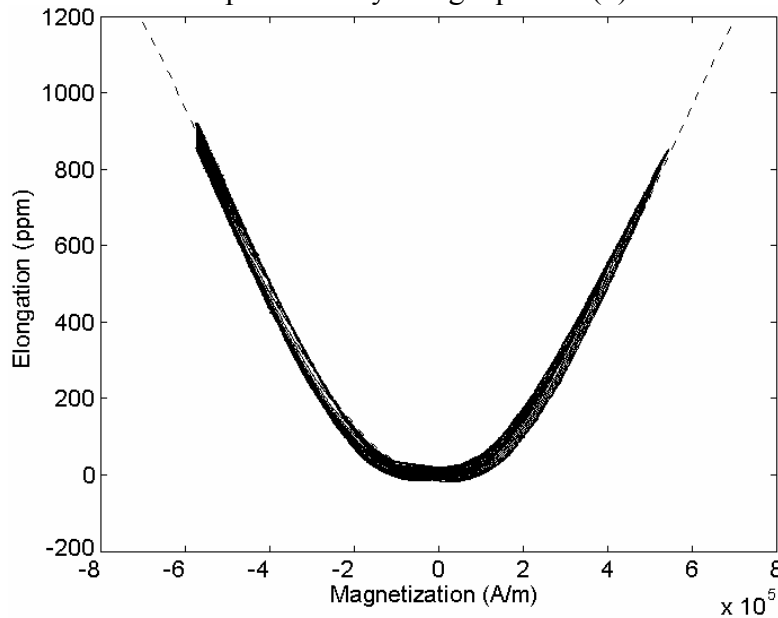


Figure 3: Elongation versus magnetization for Terfenol-D. The dashed curve is given by equation (4)

3. THE PREISACH MODEL

The Preisach model [1] is the most common and probably the most important hysteresis model in the literature. This model is not based on any physical model of hysteretic materials and it is empirical. It was developed about seventy years ago for magnetic materials.

In this model, the output is the weighted sum of the output of a continuum of hysteresis relays. The output of each relay can be either +1 or -1. In Fig. 5 a typical hysteresis relay is shown. Each relay is denoted with two parameters r and s . The parameters r and s are also known as the coercive field H_c and the interaction field H_I respectively.

The model output is:

$$y(t) = \int_0^{\infty} \int_{-\infty}^{\infty} R_{r,s}(u(t)) \mu(r,s) ds dr . \quad (5)$$

Here, $u(t)$ is the input, $R_{r,s}$ is the output of the relay, $y(t)$ is the model output and $\mu(r,s)$ is a weight function determined by experimental data.

The Preisach model is easier to understand with the introduction of Preisach plane. In the Preisach plane, the variable for horizontal axis is r and s for the vertical axis.

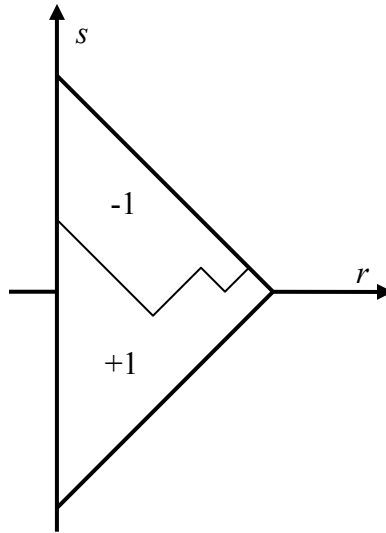


Figure 6: The Preisach plane.

Each point in this plane is in a one-to-one relation with a Preisach relay. Figure 6 shows the Preisach plane for a typical system. Because of physical reasons, the relays having large r or s values do not have a significant contribution to a change in the model output and their associated weight function is small. For simplicity, the relays outside the triangle in Fig. 6 are not considered and their weight function is assumed to be zero.

Each point inside the triangle in Fig. 6 represents a Preisach relay. The relays in +1 state are separated from the relays in -1 state with a broken line. The state of the system is represented with this broken line [14].

In order to use this model, the weight function $\mu(r,s)$ needs to be determined. There are two general approaches to this problem. You can assume a general form for $\mu(r,s)$ with some free parameters, and then try to find the values for the parameters that best match modeled output and experimental data. This approach is used below in the physics-based Preisach model.

Another approach, e.g. [15] is to assume that $\mu(r,s)$ is equal to a constant value $T_{m,n}$ in a small square defined by:

$$\begin{aligned} cm < s - r \leq c(m+1) \\ cn < s + r \leq c(n+1) \end{aligned} \tag{6}$$

where m and n are integer parameters and c is a constant. (See Fig. 7(c).) Using this approach, the model weight function is represented by a two dimensional matrix $T_{m,n}$. This reduces the number of model parameters to a finite number. Now the experimental data can be used to find a set of optimum values for these parameters.

Suppose that for a hysteretic system, a first-order descending curve between negative saturation and some input cn is obtained. Define $\Delta_{cm,cn}$ to be the system output when the input is equal to cm and the input is decreasing. The quantity $\Delta_{cm,cn}$ is obtained directly from experimental data. Fig. 7(a) shows the Preisach plane for this state. By comparing $\Delta_{cm,cn}$ and $\Delta_{c(m+1),cn}$ (Fig. 7(b)), it is seen that $\frac{1}{2}(\Delta_{c(m+1),cn} - \Delta_{cm,cn})$ is equal to the integral of the weight function $\mu(r,s)$ over the shaded area. Using a similar argument $\frac{1}{2}(\Delta_{c(m+1),c(n+1)} + \Delta_{cm,cn} - \Delta_{cm,c(n+1)} - \Delta_{c(m+1),cn})$ is equal to the integral of the weight function $\mu(r,s)$ over the square defined by Equation (6) and shown in Fig. 7(c). Since the weight function is assumed to be constant in this region, this relation yields a solution for $T_{m,n}$ which is the weight function in the square denoted by m and n :

$$T_{m,n} = \frac{1}{2c^2} (\Delta_{c(m+1),c(n+1)} + \Delta_{cm,cn} - \Delta_{cm,c(n+1)} - \Delta_{c(m+1),cn}). \tag{7}$$

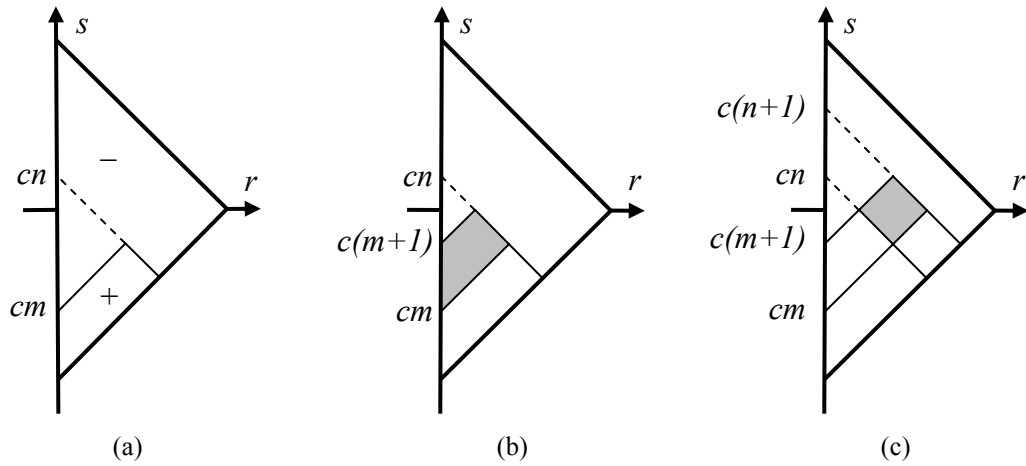


Figure 7: The Preisach plane for a first-order descending curve.

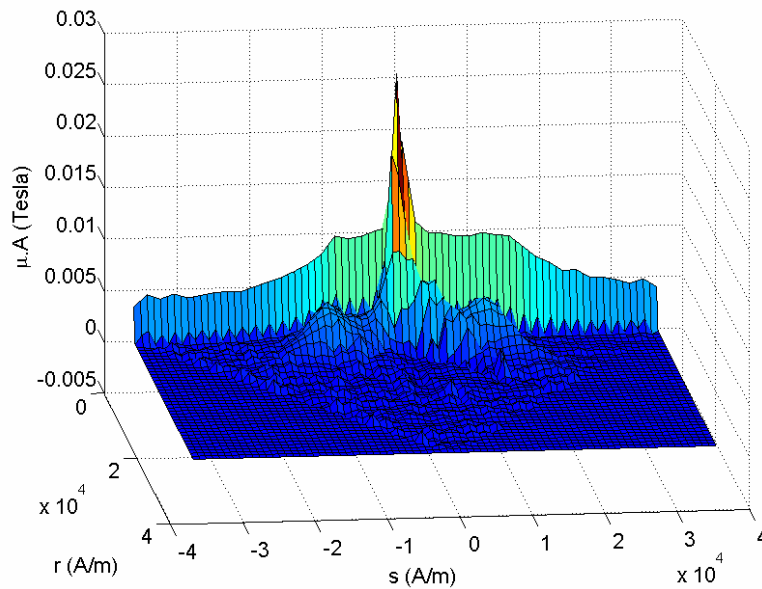


Figure 8: The Preisach weight function.

Fig. 8 displays the identified weight function $\mu(r,s)$ for the Terfenol-D sample. To verify if the Preisach model with this weight function can predict Terfenol-D behaviour accurately, an additional experiment on Terfenol-D was performed. In the beginning of this experiment, the input is oscillating between negative and positive saturation values. The amplitude of the input is decreased gradually and finally the input settles down to zero.

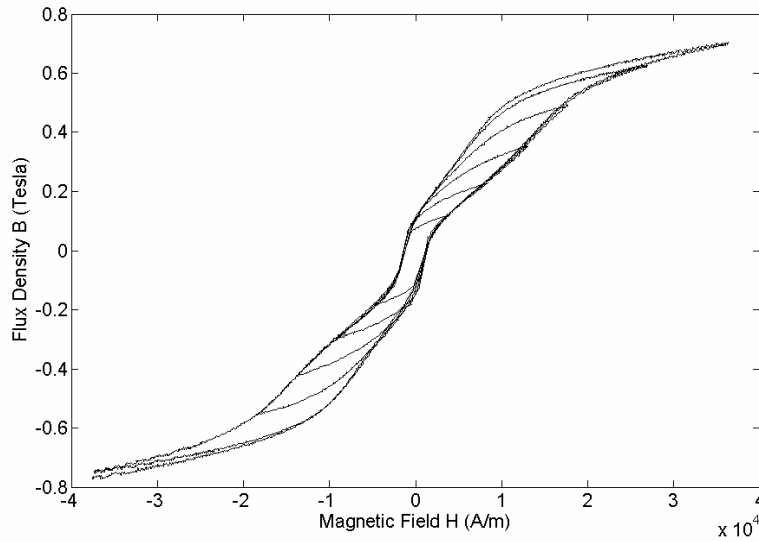


Figure 9: Experimental data for the second experiment.

Fig. 9 shows the actual output versus input for this experiment and Fig. 10 shows the Preisach model output for the same input. It is seen that the experimental data and model results are very similar, which shows the accuracy of the Preisach model prediction. The special curvature of Terfenol-D hysteresis curve is completely captured and reproduced.

The major loop of the initial experimental data and the second experiment are not identical. Small variation of experimental parameters such as temperature, etc. is likely the reason for this difference. This is believed to be the main source of error.

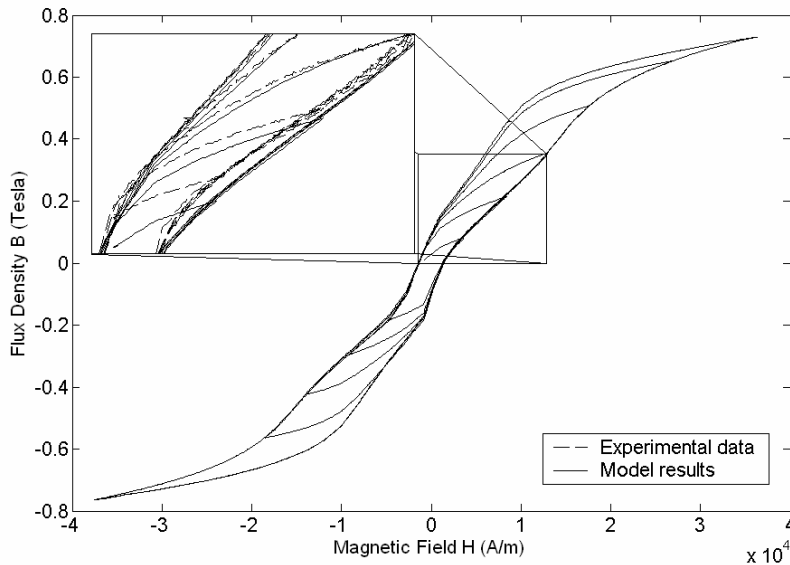


Figure 10: The Preisach model results for the second experiment.

4. THE PREISACH MODEL – A PHYSICAL APPROACH

In the physical Preisach model [3], a physical model for magnetostrictive materials is used to develop a model similar to the Preisach model. The material is assumed to be composed of a large number of weakly interacting dipoles. For each dipole, the Helmholtz free energy is modeled and a hysteron similar to Fig. 5 is obtained. Because of crystal imperfections and impurities, the dipoles are not exactly similar. By assuming a Gaussian distribution for dipole parameters, it is shown that in this model, the magnetization M is:

$$M(H) = C \int_0^\infty \int_{-\infty}^\infty \overline{M}(H, H_I, H_c) e^{-\frac{H_I^2}{b}} e^{-\frac{(H_c - \overline{H_c})^2}{b}} dH_I dH_c \quad (8)$$

where $b, \overline{H_c}$ and C are model parameters. Other distributions for dipole parameters can be assumed. In [16], a log normal distribution for coercive force H_c is suggested. In this case, the magnetization M is:

$$M(H) = C \int_0^\infty \int_{-\infty}^\infty \overline{M}(H, H_I, H_c) e^{-\frac{H_I^2}{b}} e^{-\frac{\left(\ln\left(\frac{H_c}{\overline{H_c}}\right)\right)^2}{b}} dH_I dH_c . \quad (9)$$

A piecewise constant distribution can also be used which gives a model similar to that of the previous section. The following equation defines \overline{M} :

$$\overline{M}(H, H_I, H_c) = \frac{H + H_I + R_{H_c, H_I}(H) M_R \eta}{\eta - 2Y\gamma\varepsilon} . \quad (10)$$

In this equation, η and M_R are model parameters, Y is the Young modulus for the material, ε is strain and R is the Preisach relay defined in the previous section. It is assumed that the second term in Equation (4) can be ignored and $\lambda(M) = \gamma_2 M^2$. In this case, the strain ε is given by the following equation:

$$\varepsilon = \frac{\sigma}{Y} + \gamma_2 M^2 \quad (11)$$

where σ is the stress. This model is similar to the classic Preisach model, except that for this model, the output depends on strain ε .

Root-mean-square error was computed as follows: For each value of magnetic field H , error is computed by subtracting model results from experimental data. Total model error is computed by taking the root-mean-square of these errors.

For the Terfenol-D experimental data, the best value for model parameters are found by numerically minimizing the root-mean-square error using Nelder-Mead simplex direct search method. The optimum values were found to be: $\eta = 17.766$, $b = 1.1591 \times 10^9 (A/m)^2$, $\bar{b} = 2.2540 \times 10^8 (A/m)^2$, $\overline{H_c} = -136030 A/m$, $M_R = 7417.7 A/m$ and $C = 2.0996 (m/A)^2$ for Gaussian distribution and $\eta = 0.47537$, $b = 10.837$, $\bar{b} = 1.4567 \times 10^8 (A/m)^2$, $\overline{H_c} = 0.81725 A/m$, $M_R = 8.0029 \times 10^5 A/m$ and $C = 5.5034 \times 10^{-7} (m/A)^2$ for a log normal distribution.

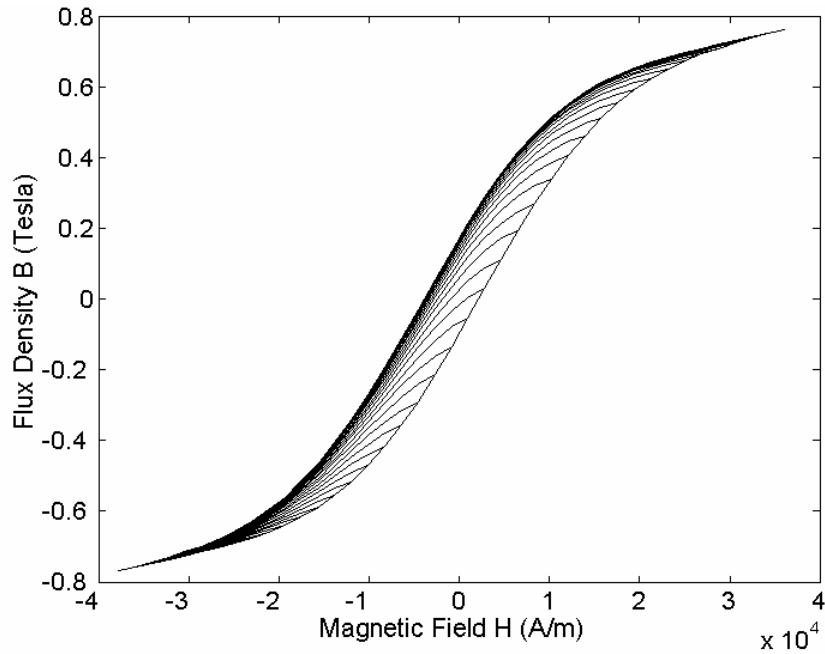
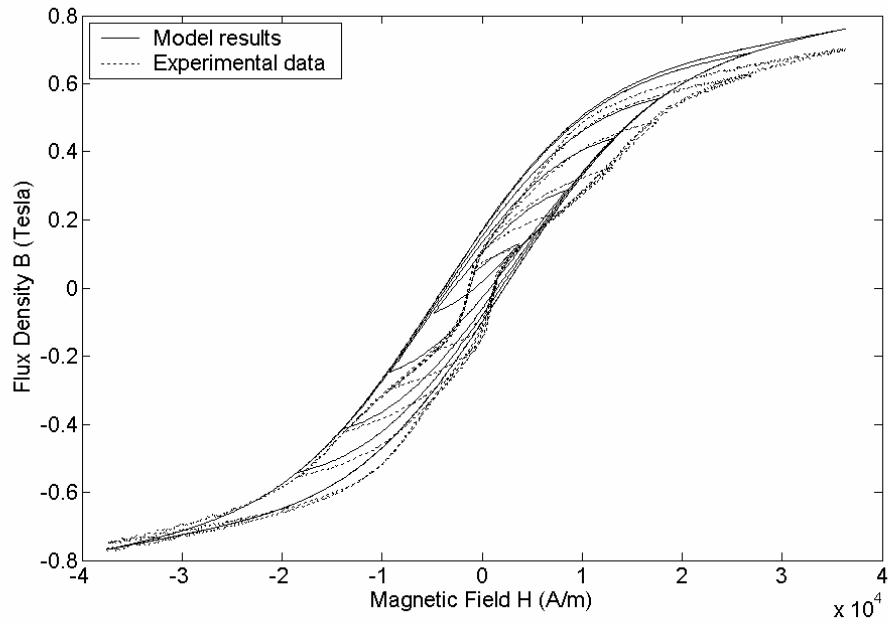
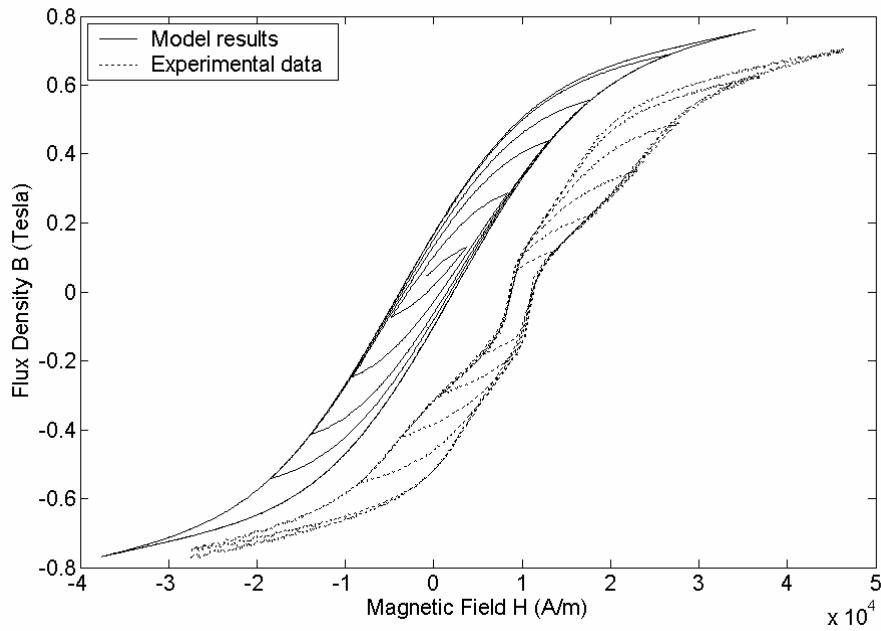


Figure 11: Minor loops produced by the physical Preisach model with Gaussian distribution.

In Fig. 11, minor loops produced by this model are shown and Fig. 12 compares the model results and experimental data for a Gaussian distribution. It is seen that the model and experimental data are close, but the curvature in the middle is not accurately captured. In Fig. 13, the model results and experimental data are compared for a log normal distribution. The result for a log normal distribution is very similar to that of the Gaussian distribution.



(a)



(b)

Figure 12: (a) The experimental data and the physical Preisach model results with Gaussian distribution. (b) The experimental results are shifted for easier comparison. The model was unable to reproduce the middle of the curve correctly.

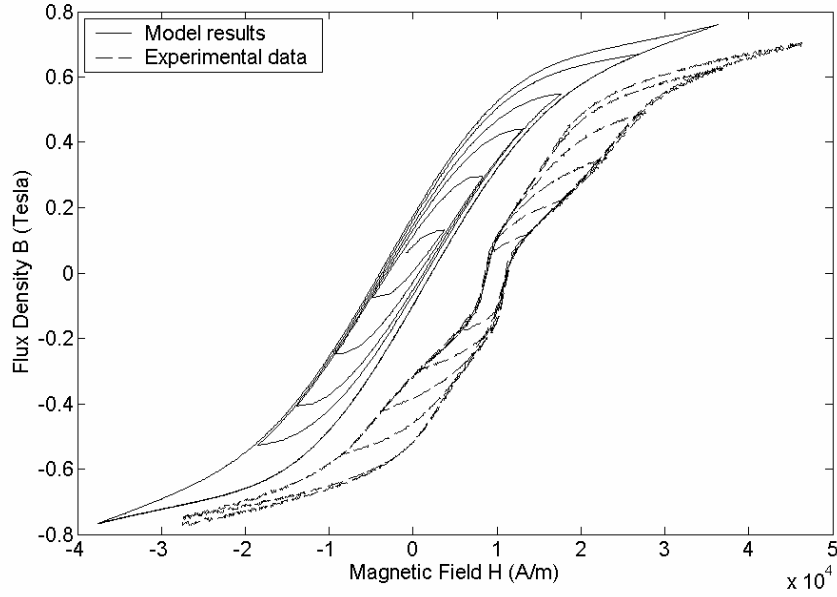


Figure 13: The experimental data and the physical Preisach model results with log normal distribution. The experimental results are shifted for easier comparison. The results are similar to that of the Gaussian distribution.

5. THE JILES-ATHERTON MODEL

The following equations describe the Jiles-Atherton model [10]:

$$\frac{dM_{irr}}{dH} = \frac{(M_{an} - M_{irr})}{\delta k - \alpha(M_{an} - M_{irr})} \quad (12)$$

$$M_{rev} = c(M_{an} - M)$$

where c , α and k are model parameters, M_{irr} and M_{rev} are the irreversible and reversible components of magnetization respectively, and $M_{rev} + M_{irr} = M$. Parameter δ is equal to +1 when H is increased and -1 when H is decreased. The parameter M_{an} is the anhysteretic magnetization. For this model, the Langevin equation is used for the anhysteretic magnetization:

$$M_{an}(H_e) = M_s \left[\coth\left(\frac{H_e}{a}\right) - \frac{a}{H_e} \right] \quad (13)$$

where a and M_s are model parameters and $H_e = H + \alpha M$.

It is seen that, in some cases, the magnetization computed by this model is increased when H is decreased, which means negative differential susceptibility. This behaviour is not physical [17]. In [17], it is suggested that in this case, $\frac{dM_{irr}}{dH}$ should be set to zero.

Some minor loops, especially small minor loops near saturation, are not produced correctly by this model. In Fig. 14, curve A is a portion of an ascending major loop. If the input is slightly decreased (Curve B) and then increased again (Curve C), the produced minor loop will not be closed. This behaviour is unphysical. To correct this problem, a solution is suggested in [18]. Define:

$$v_f = \frac{M_{irr}(H_+) - M_{irr}(H_-)}{\int_{H_-}^{H_+} \frac{M_{an} - M_{irr}}{\delta k - \alpha(M_{an} - M_{irr})} dH} \quad (14)$$

$$v'_f = \frac{M_{rev}(H_+) - M_{rev}(H_-)}{\int_{H_-}^{H_+} c \left(\frac{dM_{an}}{dH} - \frac{dM_{irr}}{dH} \right) dH}$$

where H_+ and H_- are the maximum and minimum value of magnetic field H in the minor loop respectively. In [18], it is suggested that equations (12) should be replaced by the following equations:

$$\frac{dM_{irr}}{dH} = v_f \frac{(M_{an} - M_{irr})}{\delta k - \alpha(M_{an} - M_{irr})} \quad (15)$$

$$\frac{dM_{rev}}{dH} = v'_f c \left(\frac{dM_{an}}{dH} - \frac{dM_{irr}}{dH} \right).$$

This correction can produce closed minor loops if the loops are not nested. If the minor loops are inside each other, that is, if another minor loop begins before the current minor loop closes, this correction cannot be applied to close all of the loops.

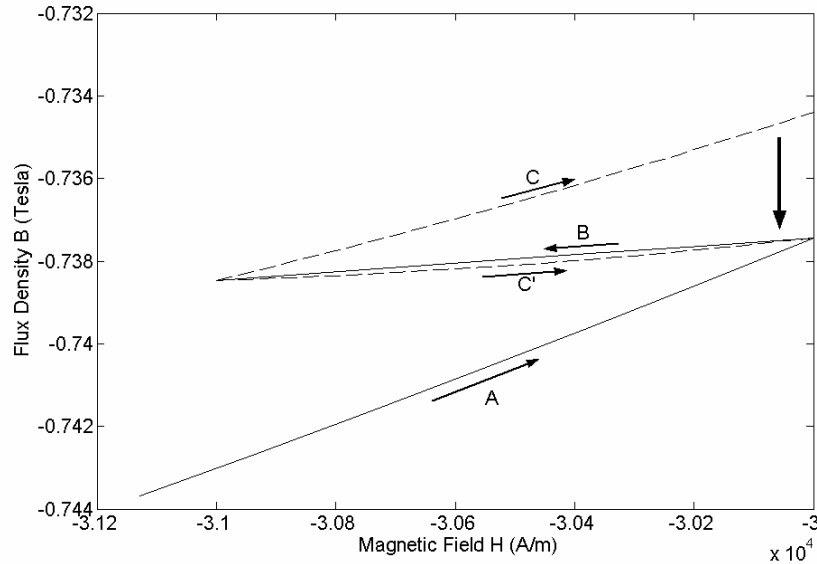


Figure 14: The closure of minor loops.

Unfortunately, Equations (14) and (15) do not yield a fast algorithm. Equations (14) and (15) are nonlinear equations that need to be solved simultaneously. This algorithm is computationally expensive.

The solution proposed in [18] is not used here. To obtain closed minor loops, each branch is scaled vertically to produce a closed loop. For example in Fig. 14, branch C is replaced by branch C'. Similar to the solution proposed in [18], the scaling is done separately for the reversible and irreversible components of magnetization. The scaling used here is computationally trivial and yields an efficient solution for closing the minor loops.

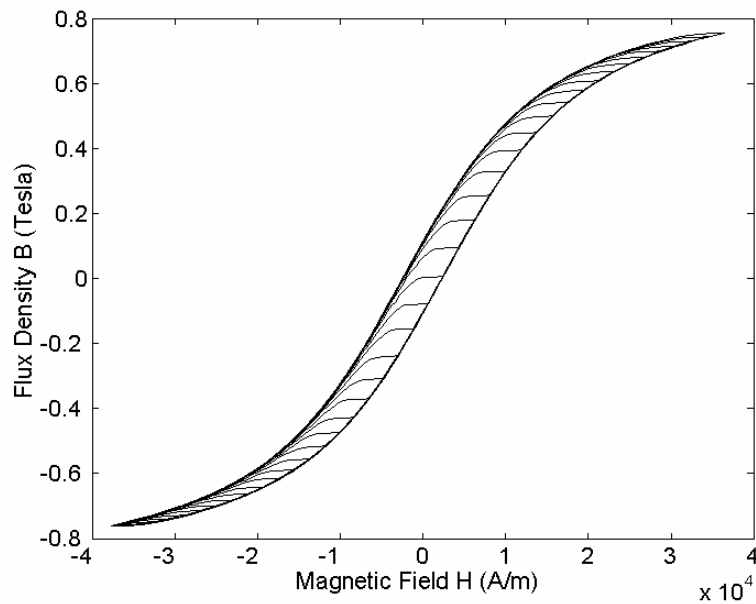
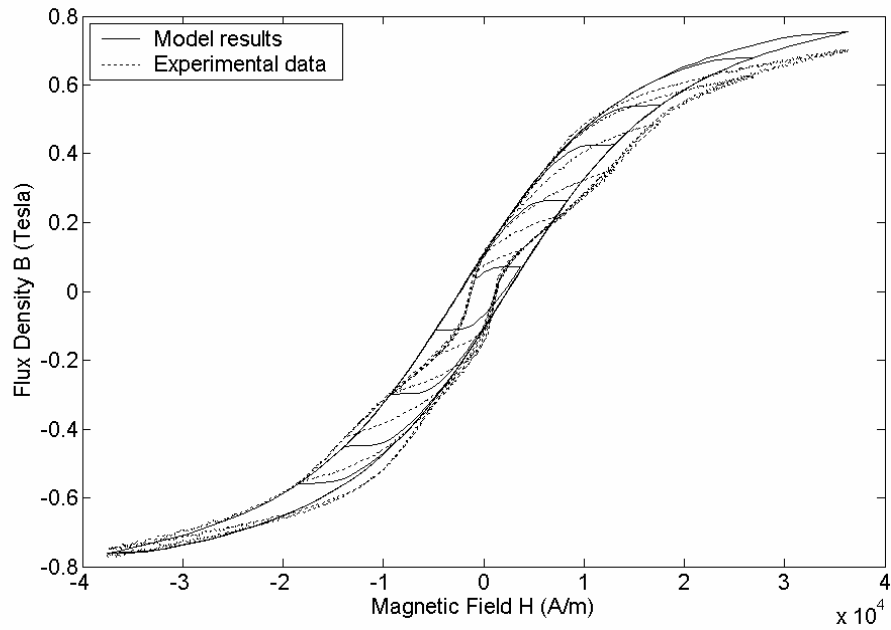
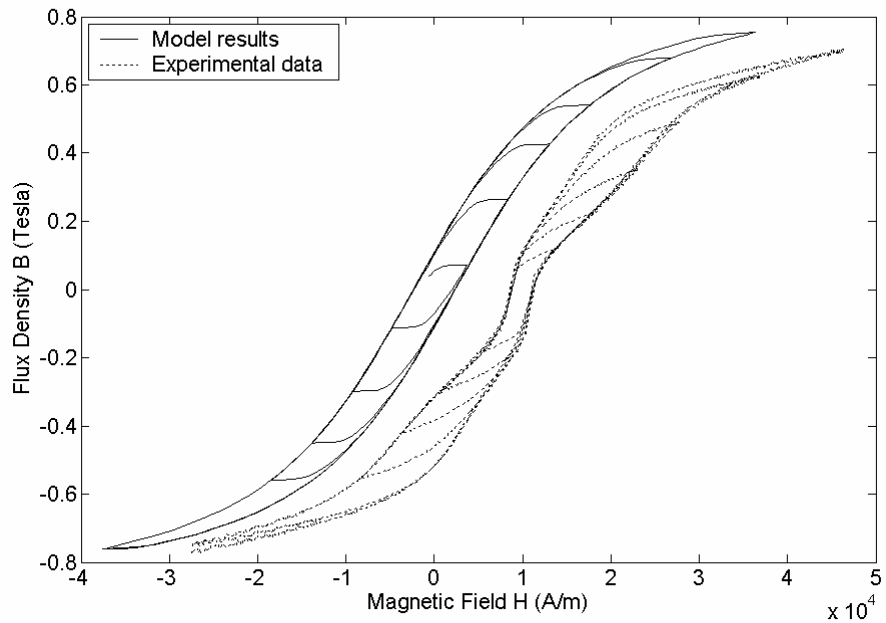


Figure 15: The minor loops produced by the Jiles-Atherton model.

The optimum model parameters were found to be: $\alpha = 1.9903 \times 10^{-8}$, $a = 6200.2 \text{ A/m}$, $M_s = 690380 \text{ A/m}$, $k = 2476.6 \text{ A/m}$ and $c = 5.7080 \times 10^{-4}$.



(a)



(b)

Figure 16: (a) The experimental data and the Jiles-Atherton model results. (b) The experimental results are shifted for easier comparison. The model was unable to reproduce the middle of the curve correctly.

In Fig. 15 the minor loops produced by this model is shown. Experimental data and model results are compared in Fig. 16. Similar to the previous section, it is seen that the model is close to experimental data, but the twisted section of the experimental data is not captured.

6. CONCLUSIONS

For all of the models discussed in this paper, experimental data is needed for model identification. This data is different for each model. The Preisach model needs at least a set of first-order descending curves. For the physics-based Preisach and Jiles-Atherton models, since they have only a few free parameters, a single loop is sufficient; e.g. the major loop.

The Preisach model could reproduce the experimental data with least error. The physical Preisach and Jiles-Atherton models had about the same accuracy; and could not capture the twisted section in the middle of the hysteresis curve.

The identification of the Preisach model was the fastest. The physical Preisach and Jiles-Atherton models were slower because of their iterative identification algorithm. The identification of the Jiles-Atherton model was particularly slow, because of the implementation issues when computing the root-mean-square error.

Minor loops have a special importance in control applications. In a typical control system, usually the major loop is not experienced, for example, it is frequently seen that the input is oscillating about an operating point. In this case, a minor loop near that point is experienced. If the oscillation amplitude decays with time, complex nested loops may be produced. For this reason, it is important to have a hysteresis model capable of handling complex minor loops for control applications. The Preisach and physical Preisach models can handle minor loops properly. The minor loop handling for the Jiles-Atherton model is not done correctly for complex cases. If Figs. 10, 12 and 16 are compared, it is seen that the minor loops for the Jiles-Atherton model join the major loop faster than the experimental data. In contrast, for the physical Preisach model, the minor loops join the major loop much slower than the experimental data. It can be said that the Jiles-Atherton model underestimates the amount of input variation required to forget past history and the physical Preisach model overestimates this amount. The Preisach model is the most accurate in this matter.

Table 1: Summary

| Parameter | The classic Preisach model | The physical Preisach model (Gaussian) | The physical Preisach model (log normal) | The Jiles-Atherton model |
|----------------------------|----------------------------|--|--|--------------------------|
| Fitting error (Tesla) | 0 | 0.0356 | 0.0322 | 0.0254 |
| Prediction error (Tesla) | 0.0172 | 0.0569 | 0.0562 | 0.0426 |
| Identification time | 1 minute | ~1 hour | ~1 hour | ~10 hours |
| Reproduction time | Instantaneous | Instantaneous | Instantaneous | ~10 seconds |
| Number of model parameters | 820 | 6 | 6 | 5 |
| Minor loop handling | √ | √ | √ | × |

In Table 1, the model comparison is summarized. Fitting error is the best error found during the model identification process and prediction error is the accuracy of the predicted output for the second experiment.

The Preisach model has 820 parameters to describe the material. This number is six for the physical Preisach model and five for the Jiles-Atherton model. The accuracy of the Preisach model is partially due to the large number of parameters. Where high accuracy is crucial, this model is the best. The Jiles-Atherton model and physical Preisach model had similar accuracy and required similar number of parameters. However, the Jiles-Atherton model does not handle minor loops properly. Furthermore, its use requires solving coupled nonlinear differential equations and is considered more computationally intensive than either Preisach model. The physical Preisach model is preferable to Jiles-Atherton. Also, as discussed in [16], the accuracy of the physical Preisach could be improved in some applications by assuming a different distribution.

REFERENCES

1. Preisach, F., "Über die magnetische nachwirkung", Zeitschrift für Physik, vol. 94, 1935, pp. 277-302.
2. Mayergoyz, I., "Mathematical Models of Hysteresis and Their Applications", Elsevier Academic Press, Amsterdam, Boston, 2003.
3. Smith, R.C., Dapino, M.J., Seelecke, S., "Free energy model for hysteresis in magnetostrictive transducers", Journal of Applied Physics, vol. 93, No. 1, 1 January 2003, pp. 458-466.
4. Ktena, A., Fotiadis, D.I., Berger, A., Massalas, C.V., "Preisach Modeling of AFC Magnetic Recording Media", IEEE Transactions on Magnetics, Vol. 40, No. 4, July 2004, pp.2128-2130.
5. Gorbet, R.B., Morris, K.A., Wang, D.W.L., "Passivity-Based Stability and Control of Hysteresis in Smart Actuators", IEEE Transactions on Control System Technology, Vol. 9, No. 1, January 2001, pp. 5-16.
6. Smith, R.C., Dapino, M.J., "A Homogenized Energy Model for the Direct Magnetomechanical Effect", Center for research in scientific computation, CRSC-TR05-31, <http://www.ncsu.edu/crsc/reports.htm>.
7. Tan, X., Barasa, J.S., "Modeling and control of hysteresis in magnetostrictive actuators", Automatica, Vol. 40, No. 9, September 2004, pp. 1469-1480.
8. Smith, R.C., Hatch, A.G., "Parameter estimation techniques for a class of nonlinear hysteresis models", Inverse problems, Vol. 21, No. 4, August 2005, pp. 1363-1377.
9. Smith, R.C., Hatch, A.G., Mukherjee, B., Liu, S., "A Homogenized Energy Model for Hysteresis in Ferroelectric Materials: General Density Formulation", Journal of intelligent material systems and structures, Vol. 16, No. 9, September 2005, pp. 713-732.
10. Jiles, D.C., Atherton, D.L., "Theory of ferromagnetic hysteresis", Journal of Magnetism and Magnetic Materials, vol. 61, 1986, pp. 48-60.

11. Sablik, M.J., Jiles, D.C., "Coupled Magnetoelastic Theory of Magnetic and Magnetostrictive Hysteresis", IEEE Transactions on Magnetics, vol. 29, No. 3, July 1993, pp. 2113-2123.
12. Dapino, M.J., Smith, R.C., Faidley, L.E., Flatau, A.B., "A Coupled Structural-Magnetic Strain and Stress Model for Magnetostrictive Transducers", Journal of Intelligent Material Systems and Structures, Vol. 11, February 2000, pp. 135-152.
13. Jiles, D.C., "Theory of the magnetomechanical effect", Journal of Physics D: Applied Physics, vol. 28, No. 8, 14 August 1995, pp. 1537-1546.
14. Gorbet, R.B., Morris, K.A., Wang, D.W.L., "Control of hysteretic systems: A state-space approach", *Learning, control and hybrid systems*, Edited by Yutaka Yamamoto, Shinji Hara, Bruce A. Francis and M. Vidyasagar, Springer-Verlag, New York, 1998, pp. 432-451.
15. Valadkhan, S., *Modeling of magnetostrictive materials*, MSc. Thesis, University of Waterloo, Department of Mechanical Engineering, 2004, pp. 86-91.
16. Smith, Ralph C., *Smart material systems: Model development*, Society of Industrial and Applied Mathematics, Philadelphia, 2005.
17. Jiles, D.C., Thoenke, J.B., Devine, M.K., "Numerical determination of hysteresis parameters for the modeling of magnetic properties using the theory of ferromagnetic hysteresis", IEEE Transactions on Magnetics, vol. 28, No. 1, 1992, pp. 27-35.
18. Jiles, D.C., "A self consistent generalized model for the calculation of minor loop excursions in the theory of hysteresis", IEEE Transaction on Magnetics, vol. 28, No. 5, September 1992, pp. 2602-2604.